Journal of Marine Science and Technology (2019) 24:902–916
https://doi.org/10.1007/s00773-018-0595-6

ORIGINAL ARTICLE

A non-contact docking system for charging and recovering autonomous underwater vehicle

Ri Lin[1] · Dejun Li[1] · Tao Zhang[1] · Mingwei Lin[1]

Received: 25 January 2018 / Accepted: 4 September 2018 / Published online: 20 September 2018

Abstract
To improve the observation capability of the ocean, the combination of the static cabled ocean observatory network and the dynamic autonomous underwater vehicle has attracted more and more attention. In this paper, a non-contact docking system for the autonomous underwater vehicle is developed to combine the advantages of the cabled ocean observatory network and the autonomous underwater vehicle. The system includes both acoustic and optical navigation, underwater wireless communication, non-contact power transfer, and monitoring and controlling of the docking system. This docking system was verified by sea trials at depths of 50 and 105 m. The autonomous underwater vehicle successfully docked 11 times, during which non-contact power transfer and wireless communication were completed. The charging power reached 682 W, with a total efficiency of 78.5%, and the efficiency of the power transfer unit was 92%. The rate of wireless data transfer reached 3.1 MB/s. For the first time, this docking system has realized complete homing and docking navigation, wireless communication and charging in a water depth of more than 100 m, thus establishing a good foundation for the combination of the cabled ocean observatory network and autonomous underwater vehicles.

Keywords Docking system · Autonomous underwater vehicle · Underwater wireless communication · Underwater non-contact power transfer · Sea trial

1 Introduction

More researchers have become committed to the exploration and development of the ocean, where many biological and mining resources exist. The cabled ocean observatory network (COON) has received worldwide attention in both real-time and long-term observation [1]. However, due to the fixed location of the COON, only static observations can be made in a specific area. In addition, autonomous underwater vehicles (AUVs) have drawn widespread attraction in recent years due to their outstanding ability to observe a large subsea area [2]. However, they cannot execute a long-term underwater mission because of their limited energy storage [3]. Hence, an underwater docking system was developed to provide underwater charging and recovery for AUVs without the help of a mother ship [4]. Much evolutionary work has been conducted to complete and enhance such a docking system. Except for power transfer, the technologies of the docking system include establishing the docking station, underwater communication and AUV homing and docking navigation [5].

Docking systems can be divided into the pole and latch type [6], aircraft landing type [7], pyramid type [8] and funnel type [9] according to their docking station structures. Among these types, the funnel-type docking system can reduce the accuracy demand of AUV navigation and requires less modification. The WHOI REMUS100 AUV docking system [10–12], the MBARI's 54-cm-diameter (21-in) AUV docking system [13, 14], the FAU 12.5-in AUV docking system [15] and the EURODOCKER docking system [16] have all adopted the funnel-type form, with a funnel-type entrance installed in front of the docking station. With this feature, the AUV can be guided into the docking station easily as long as the AUV enters the entrance.

In addition, the underwater docking systems can be classified into the physical-contact and non-contact types according

Electronic supplementary material The online version of this article (https://doi.org/10.1007/s00773-018-0595-6) contains supplementary material, which is available to authorized users.

✉ Dejun Li
li_dejun@zju.edu.cn

[1] The State Key Laboratory of Fluid Power and Mechatronic Systems, Zhejiang University, Hangzhou 310027, China

to the methods of power and data transmission that are used. The former adopts physical-contact methods such as underwater wet-mate connectors to accomplish underwater signal and power transmission, whereas the latter uses non-contact methods such as electromagnetic coupling and wireless communication. For traditional physical-contact methods, wet-mate connectors are commonly used. However, when wet-mate devices are used in docking systems, some drawbacks appear. First, a precise alignment between the plug and the socket is needed, which is difficult to obtain in an underwater environment. Second, a special device is required to offer the driving force to push the plug into the socket, which makes the structure more complex. Third, when the wet-mate connector is employed in the deep sea for a long time, it needs strong water- and pressure-proof capabilities and requires special maintenance. Compared with physical-contact methods, non-contact technology has the advantages of a simple structure, reliable operation, and non-corrosion, which make it especially suitable for long-term underwater missions [17]. A previous study [18] introduced a kind of inductive coupling power transmission device that adopts the cone-type coupling coils with a magnetic core and realizes non-contact power transmission with a power of 500 W and efficiency over 90%. Tokyo University has developed a system for charging a deep-sea mobile platform. According to their experimental results in the pool, the transmission power of this system reaches 400 W, with an efficiency of more than 77% for the power transmission device [19, 20]. FAU developed a docking system that uses the insertion type of non-contact power transmission device. The transmission power of the device can reach 1000 W at an input voltage of 50 V, and its efficiency is above 80% [15]. Other studies [21, 22] introduced a kind of underwater non-contact power and data transmission interface that can transmit electricity and signals through electromagnetic coupling technology. Its electricity output reaches 200 W, with an efficiency of 79%, and its communication rate is 10 Mb/s.

The development of these technologies has greatly improved the endurance of AUVs and reduced the cost of recovery. However, the underwater docking system for an AUV has not reached the stage of practical application, even after more than a decade of development. Much research thus remains to be done. In this paper, a non-contact docking system designed to connect to the COON is developed based on the research foundation of Shi et al. [23, 24]. Underwater acoustic and optical navigation are combined to achieve AUV homing and docking. High-frequency electromagnetic wave communication is adopted to realize underwater wireless communication. The inductive coupling power transfer (ICPT) technology is applied to establish the non-contact power transmission system. With the embedded PC as the core, a monitoring and control system is constructed.

The rest of this paper is organized as follows. Section 2 describes the overall configuration of our non-contact docking system. Section 3 discusses the principle of underwater wireless communication and states the implementation of the wireless communication system. Section 4 describes the inductive coupling power transfer system utilized to implement wireless power transfer in detail. Section 5 briefly introduces vehicle navigation and control that includes acoustic and optical navigation to control the AUV homing and docking. Section 6 introduces a control and monitoring system that makes the systems above work correctly. Section 7 discusses the results of the sea trial.

2 Overall configuration

The docking system described in this paper is composed of a docking station and an AUV. Since the docking station is the main part of this system, it is emphasized in this article.

In Fig. 1, the structure of the docking station is divided into two parts: the pedestal and the mainframe. The pedestal is the main load-bearing part of the docking station. It makes the deployment smooth and reduces the influence of ocean currents. The mainframe is the core structure of the docking station and is interiorly equipped with a guidance and lock structure, a circuit chamber, navigation devices, data acquisition devices, and wireless communication devices. The mechanical structures of the frame mainly include the guidance and lock structure and the circuit chamber where the control circuits are installed.

The guidance and lock structure is composed of a funnel-type entrance, nylon fastener, and electromagnetic lock. The center of this entrance is 3.25 m from the bottom. The inner and outer diameters of the entrance are 300 mm and 1200 mm, respectively. The cone angle of the funnel-type entrance is 60°. This entrance has a fence shape to reduce the influence of ocean currents on the docking station. The back of the funnel-type entrance is installed with a nylon fastener, where the transmitter coil and the antenna are fixed. After the AUV has docked successfully, it is latched by the electromagnetic lock. The electromagnet provides a suction of 110 N, which is sufficient to lock the AUV firmly in the station, according to our test results. In the case of good docking, the transmitter coil aligns well with the pickup coil, and the distance between the two antennas is less than 7.5 cm, which allows wireless communication.

The electrical connection and communication of the docking system are shown in Fig. 2. The docking station is connected to the COON by the optical composite cable, the photoelectric conversion chamber and the watertight cable. Then, it obtains a 375 V direct current (DC) supply and Ethernet communication from the COON. The 375 V power is converted into different voltages to supply power to the embedded PC and other devices in the docking station. The embedded PC and these devices are linked to a switch

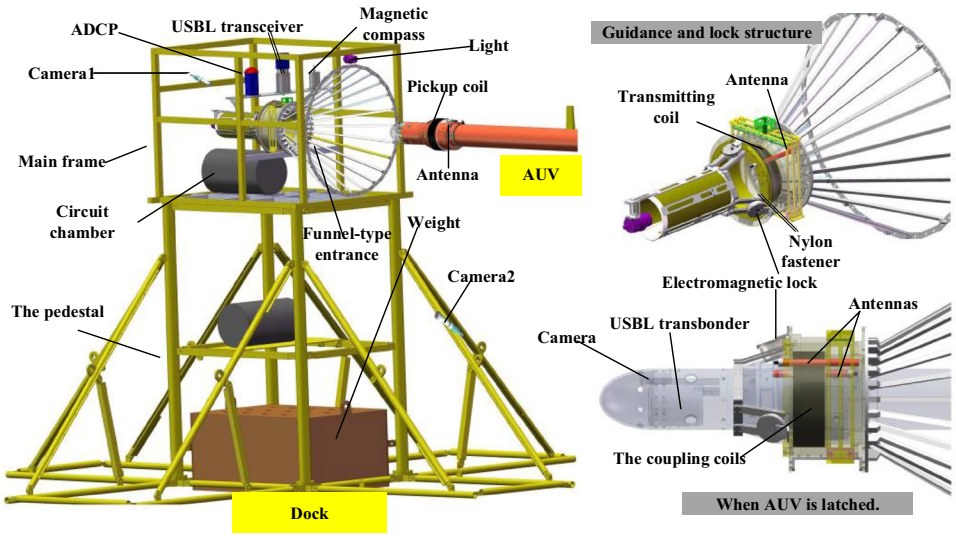

Fig. 1 Overall configuration of the docking system

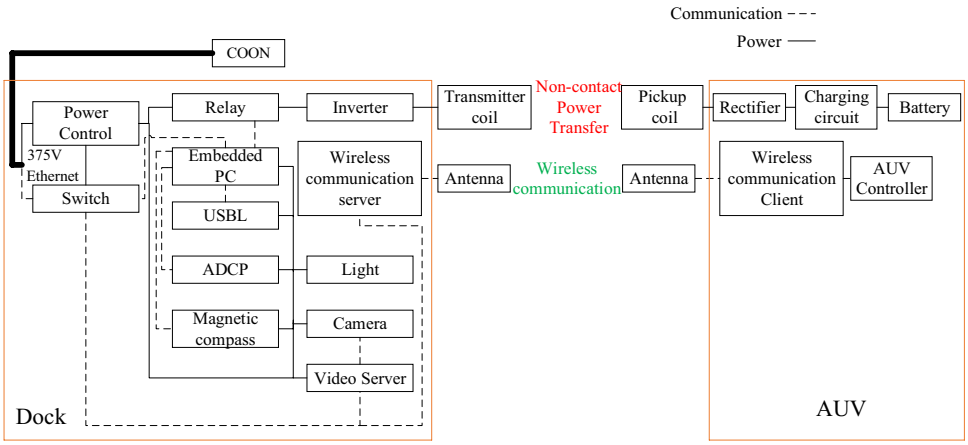

Fig. 2 Electrical connection and communication in the docking system

and then communicate with each other via an ethernet. An ultrashort baseline (USBL), depth sensor, magnetic compass, light, cameras, and acoustic Doppler current profiler (ADCP) are the external devices controlled by the embedded PC. The wireless link consists of routers and antennas on the docking station and the AUV realizes underwater wireless communication. The inverter converts the direct voltage into high-frequency voltage, and power is transferred from the docking station to the AUV through the coupling coils. After being rectified and charged, electrical energy is stored in the battery. According to their functions, these devices in our docking system can be sorted into a non-contact power transfer system, a wireless communication system, a navigation system and a control and monitoring system.

3 Wireless communication system

After the AUV is latched in the docking station, the data collected by the AUV is uploaded through a wireless communication system, and at the same time the docking station updates a new tasks file to the AUV. The wireless underwater communication can be realized by optical communication, acoustic communication or electromagnetic waves [25–27]. Optical communication is susceptible to water quality, and acoustic communication is weak in communication rate. However, electromagnet wave communication has the characteristic of a high communication rate over a short distance. Hence, high-frequency electromagnetic wave communication technology is applied to realize submerged data communication.

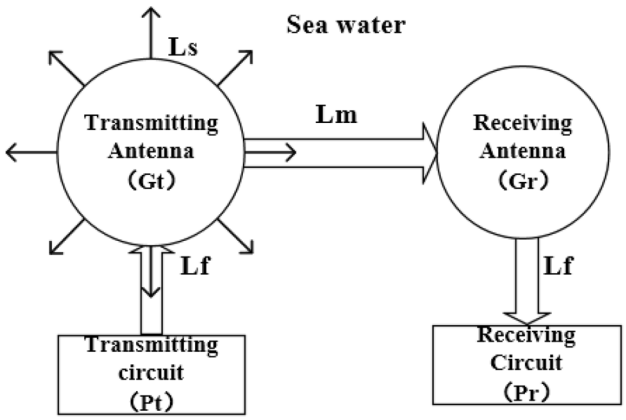

Fig. 3 Attenuation of the signal in the transmitting path

3.1 Signal propagation path and attenuation analysis

High-frequency electromagnetic waves are greatly attenuated in seawater [28–30], so the penetration distance must first be evaluated to ensure that high-frequency electromagnetic wave communication can be applied in this docking system. The signal transmission path and attenuation in the path are shown in Fig. 3.

The power balance equation in the propagation is

$$P_t - P_r = L_m + L_s + L_f + L_b - G_t - G_r, \tag{1}$$

where P_t is the power of the transmitting antenna; P_r is the power of the receiving antenna; L_f, L_m and L_s denote the loss among the feeder line and the connector, the medium loss and the space loss, respectively; L_b is the link budget, and its value should be greater than 10 dB in normal working situations; G_t is the gain when the signal passes through the antenna; G_r stands for the gain obtained by the receiving antenna.

The medium loss is calculated as

$$L_m = 20 \lg e^{\alpha d}. \tag{2}$$

The calculation of the space loss is

$$L_s = 20 \lg \left(\frac{2d}{\beta} \right), \tag{3}$$

where α is the attenuation coefficient in the medium and β is the phase constant. They are related to the frequency f of the electromagnetic wave, the relative permeability μ of the medium, the conductivity γ and the dielectric constant ε. Their expressions are

$$\alpha = 2\pi f \sqrt{\frac{\varepsilon \mu}{2} \left[\sqrt{1 + \left(\frac{\gamma}{2\pi f \varepsilon} \right)^2} - 1 \right]}, \tag{4}$$

$$\beta = 2\pi f \sqrt{\frac{\varepsilon \mu}{2} \left[\sqrt{1 + \left(\frac{\gamma}{2\pi f \varepsilon} \right)^2} + 1 \right]}. \tag{5}$$

A router linked to the external 3 dBi omnidirectional antenna is used in this paper. According to the actual working conditions, there are $P_t = 17$ dBm, $P_r = -85$ dBm, $G_r = G_t = 3$ dBi and $L_f = 1$ dBm. The relationship between the link budget L_b versus the distance d between antennas at different frequencies can be found in Fig. 4.

In this paper, wireless devices with a working frequency of 2.4 GHz are utilized. The attenuation of electromagnetic waves in seawater is great, but the link budget of the wireless devices is still above the allowance when the distance between antennas is less than 8 cm (Fig. 4). So, the distance designed between antennas in the docking station and the AUV should be less than 8 cm.

3.2 Network architecture

In Fig. 5, the routers, the embedded PC controller, the host computer terminals, the controller in the AUV, and the optical navigation module are in line with IEEE 802.11a/b/n specifications. In addition, they are linked together via Ethernet communication, forming a simple LAN where all network devices are on the same IP network segment, so that any device in this network can be accessed via the host computer terminals.

3.3 Laboratory test

This system's network architecture (Fig. 5 Block diagram of wireless communication.) was applied to simulate real conditions to obtain stable transmission rates at different

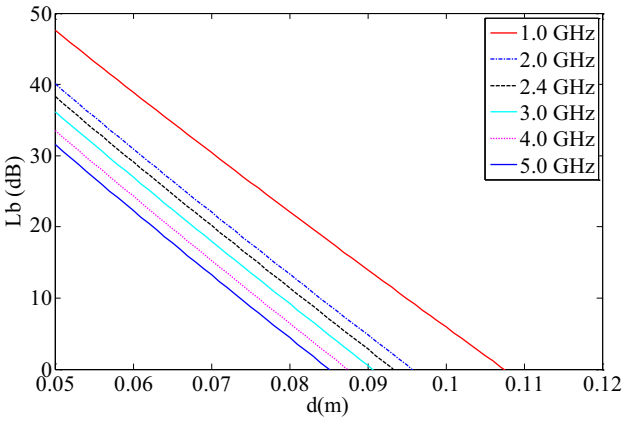

Fig. 4 The link budget varies with the distance between antennas in different working frequencies

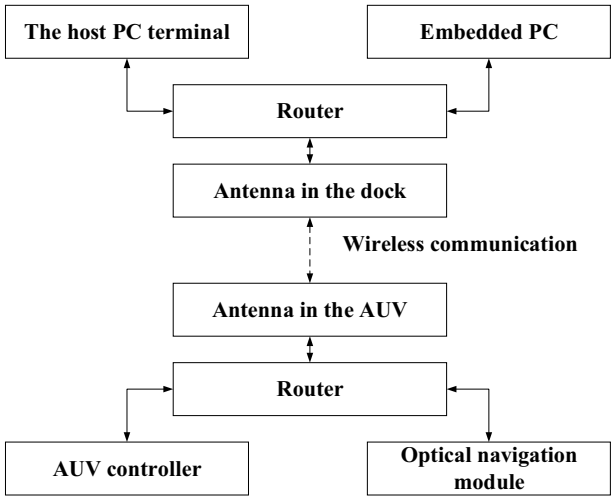

Fig. 5 Block diagram of wireless communication

antenna distances in laboratory, so that the possibility of underwater electromagnetic communication can be analyzed. The two routers connected the antenna and the laptops simulating the docking station and the AUV. Tests were conducted in a simulated seawater environment, and the large files were used to transmit between the two laptops under the network architecture to test the stable wireless transmission rate. The result is seen in Fig. 6. It is found that when the distance of the two antennas is in the range of 35–47 mm, the transmission rate has no obvious relationship with the distance. However, when the distance is above 47 mm, the transmission rate drops with increased distance, especially if the distance exceeds 55 mm. It is observed that the wireless network connection is interrupted when the distance between two antennas is larger than 75mm. Therefore, the distance between the two antennas is designed less than 75 mm to guarantee the transmission rate (assume that the AUV latched in the docking station has a normal roll angle that between − 30° and 30°).

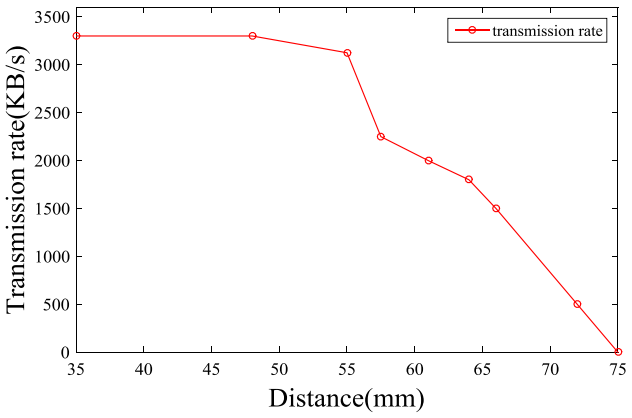

Fig. 6 Underwater wireless transmission rates test in laboratory

4 Non-contact power transfer system

The non-contact power transfer system is an important system that greatly improves the endurance of an AUV. Wireless forms of power transfer include LED/laser transfer, capacitive transfer and inductively coupled power transfer (ICPT) [31]. However, ICPT is most widely used because it is a relatively mature and reliable form of non-contact power transfer. In this docking system, an ICPT system is applied to realize underwater wireless charging.

4.1 Coupling coils

A new type of coreless coil with large diameter is designed for the ICPT system according to the structure of the docking station and the AUV. The pickup coil is fixed outside the AUV, and the transmitter coil is fixed in the nylon fastener (Fig. 1). Once the AUV parks in the docking station, the two coils realize the coupling well, which is a convenient method to utilize underwater. Moreover, it does not use the magnet core, so core loss does not exist in this ICPT system. To reduce the alternating current (AC) resistance caused by the skin effect and proximity effect, the coils in this system are wound with Litz wire with a diameter of 1.5 mm. They are sealed by epoxy resin so they can be utilized underwater safely. The parameters of the coupling coils are shown in Table 1.

4.2 ICPT modeling

ICPT systems tend to have large leakage inductance with a relatively low power factor, which is compensated by capacitors to increase the transfer capacity. Several types of compensation topologies have been previously investigated, with different characteristics suggested for various applications [32–34]. In this paper, to ensure the reliability of the system,

Table 1 Parameters of the coils

Basic parameters	Primary coil	Secondary coil
Diameter (mm)	300	282
Turns	50	40
Inductance (μH)	983	611
Resistance (Ω)	0.72	0.53
Frequency (kHz)	50	
Coupling coefficient	0.835	

compensation with a series capacitor in the secondary side is selected and it is called NS topology, where *N* denotes none capacitor compensated in the primary side, *S* denotes a serial capacitor compensated in the secondary side.

The simplified ICPT system based on NS topology is shown in Fig. 7. Because the resistance of the two coils is very small compared with the load, its effect is negligible. The AUV charging circuit and battery pack are equivalent to a resistance load R_0. Vg is a 375 V DC voltage source. V1 is a square wave with a voltage of 375 V generated by the inverter, which is a phase-shift full bridge inverter whose switching frequency is f_0; L_p and L_s denote the inductance of the transmitter and pickup coil, respectively. C_s denotes the secondary serial capacitor. C_o denotes the output filter capacitor connected to the rectifier. *M* denotes the mutual inductance of the coupling coils.

The battery we used is charged with a CC–CV strategy. The charging current is 15 A under a constant current charging state, and the charging voltage is 48 V under a constant voltage charging state. Its charging power ranges from 500 to 720 W. So the system we designed is to realize a charging power from 500 to 720 W. The output voltage V_o of the ICPT should be between 200 and 350 V according to the input need of the buck module connected to the secondary side and battery. Since the efficiency of the buck module we use is constant at 0.85, and the output power of the ICPT system should be in the range of 588–847 W.

According to a previous study [35], some parameters in Fig. 7 have the following relationship:

$$\frac{V_o}{V_L} = \frac{2\sqrt{2}}{\pi}, \tag{6}$$

$$R_{eq} = \frac{V_L}{I_L} = \frac{8}{\pi^2} R_0. \tag{7}$$

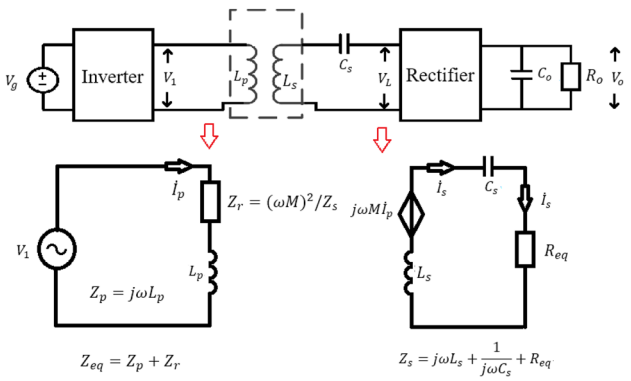

Fig. 7 Analysis of the ICPT system (the top is the simplified ICPT system, the bottom is the equivalent circuit of the ICPT)

The ICPT circuit can be equivalent to the primary circuit loop, whose equivalent impedance is

$$Z_{eq} = Z_p + Z_r = Z_p + \frac{{\omega_0}^2 M^2}{Z_s}, \tag{8}$$

where ω_0 is equal to $2\pi f_0$. Generally, the reactance of the secondary side is set to zero to improve the power factor in NS topology, so C_s is defined as follows:

$$C_s = 1/\omega_0^2 L_s. \tag{9}$$

Because the ICPT system is an open loop system, the output voltage of the secondary loop will change with the load when it is resonant. To ensure normal charging, the output voltage of the ICPT system should be stabilized at 200–350 V. The output voltage gain M_V is

$$M_V = \frac{V_o}{V_g} = \frac{1}{\sqrt{Q^2 k^2 n^2 + \frac{1}{k^2 n^2}}}. \tag{10}$$

In the formula (10), Q is the load quality factor, with $Q = \omega_0 L_p / R_e$, and k is the coupling coefficient, with $k = M/\sqrt{L_p L_s}$; n stands for the effective turn ratio, and $n = \sqrt{L_s/L_p}$. However, the formula (10) is derived from the equivalent model that only considers the fundamental component of the voltage waveform and does not consider the dead band time Δt or phase-shifting angle δ of the full bridge inverter impact on the output voltage. Therefore, this paper adds two parameters β_1 and β_2 to compensate for the input voltage and load resistance in the equivalent model based on formula (10). The expression of the voltage gain function after compensation is

$$M_V = \frac{\beta_1}{\sqrt{\left(\frac{\omega_0 L_p}{\beta_2 R_{eq}}\right)^2 k^2 n^2 + \frac{1}{k^2 n^2}}}. \tag{11}$$

In the laboratory test, we sampled the output voltage of ten different loads in the ICPT system and then fit the curve of the output voltage versus the load. Using MATLAB, the best fitting curve is obtained, and the β_1 and β_2 in Eq. 11 are, respectively, 1.160 and 2.544. It is worth mentioning that in this test, the switching frequency f_0 is 50 kHz, the dead time Δt of the inverter is 560 ns, and the phase-shifting angle δ is 0.25%. Because the output power of the ICPT system should be 588–847 W, it can be calculated by Eq. 11 that the equivalent resistance ranges from 55 to 110 Ohm (Fig. 8). The output voltage of the secondary side also meets the design requirement within this range of resistance.

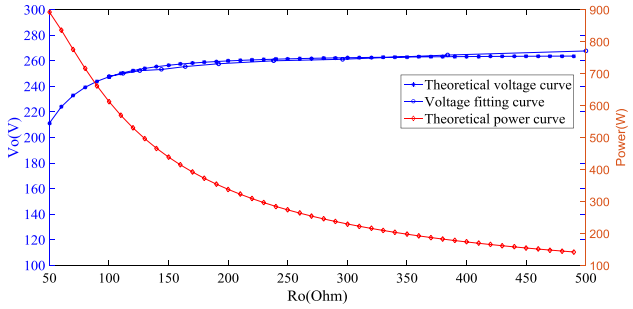

Fig. 8 The system output voltage fitting curve and output voltage power simulation curve

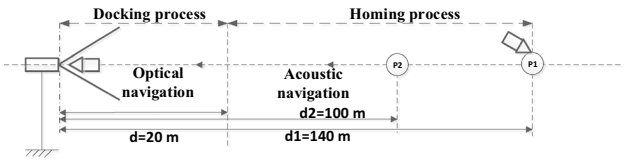

Fig. 9 AUV homing and docking schematic diagram

5 Vehicle navigation and control

Successful homing and docking are prerequisites for the follow-up tasks of the docking system, so precise navigation is crucial. The homing and docking process of the AUV is shown in Fig. 9. P1 and P2 are the two points in the dock centerline at the AUV coordinates. The AUV flies to point P1 using the extended Kalman filter (EKF) from arbitrary points, and it then starts the homing process. Point P1 is where the AUV can receive the USBL signal. The AUV first travels to point P2 using the EKF, during which the AUV continually adjusts its heading angle and depth. When it arrives at P2, it has a good heading toward the docking station. Since the voyage at this process does not require high precision, the AUV can travel without USBL. When the AUV reaches P2, it starts acoustic navigation with cross-track error control. The USBL signal is combined in the EKF to update the AUV location during the homing process. When the distance between the AUV and docking station is less than 20 m, the AUV prepares the docking process via optical navigation.

5.1 Acoustic navigation

The acoustic navigation system includes the USBL, Doppler velocity log (DVL) in the AUV, depth sensors, magnetic compass in both the docking station and the AUV. Among them, USBL consisting of a transponder and a transceiver is the most crucial positioning equipment [36]. The install position of the transponder and the transceiver affects the position accuracy. If the transceiver is installed on the AUV, the attitude information of AUV is utilized when the positioning information is converted from the body coordinate to the inertial coordinate. The attitude information of AUV is measured by the electronic magnetic compass (TCM 5), so the positioning result of the transceiver is affected by the accuracy of the magnetic compass. In addition, when the attitude data and the positioning result are not obtained simultaneously, errors will also appear in position calculation. But if the transceiver was installed on the docking station, the attitude of the docking station is constant which means that it does not have to be collected all the time. So, the accuracy of positioning will be improved. Therefore, to improve the accuracy of positioning, the transceiver is installed above the funnel-type entrance in the docking station and the transponder is installed on the head of the AUV. After receiving the positioning information of the AUV, the AUV integrates it into the EKF navigation system. These sensors work together to control the AUV in the depth and horizontal plane. The proportion-integral-derivative (PID) controller is adopted because it is robust and easy to implement.

The definition of each parameter during homing and docking is seen in Fig. 10 which contains three coordinates: the earth coordinate, the AUV coordinate and the DOCK coordinate. The origin of the DOCK coordinate is $(x_{\text{dock}}, y_{\text{dock}})$ in the earth coordinate, and the heading angle of the DOCK is φ_{dock}. The origin of the AUV body coordinate is $(x_{\text{AUV}}, y_{\text{AUV}})$ in the earth coordinate, and the heading angle of the AUV is ψ_{AUV}; Δy denotes the cross-track error or said distance between the AUV and the dock centerline; $\Delta\psi_{\text{AUV}}$ denotes the angle between the AUV and the dock centerline.

The depth control is formed by two-stage PID in series, the PID control of the depth-to-pitching angle and the PID

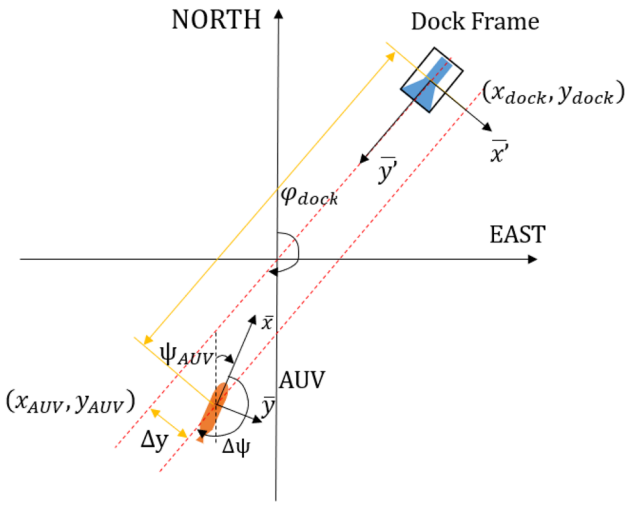

Fig. 10 Parameter definitions in AUV homing progress [13]

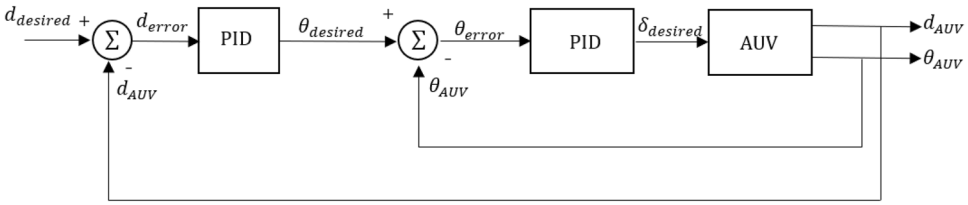

Fig. 11 The depth control of the AUV

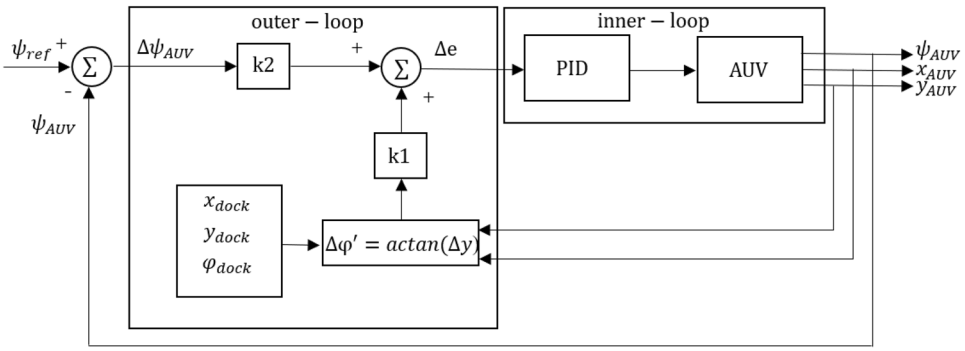

Fig. 12 PID control in the horizontal plane homing process

control of pitch-to-rudder angle (Fig. 11). Where θ_{AUV} is the pitch angle of the AUV, $\theta_{\mathrm{desired}}$ is the desired pitch angle; d_{AUV} is the current depth of the AUV; d_{desired} is the desired depth; and δ_{error} is the rudder angle of the elevator. In the depth control, whether the depth error satisfies the control requirements in the vertical direction is the only thing to consider.

The AUV in this docking system is an under-driven AUV that cannot directly eliminate the cross-track error during homing. The cross-track error can only be eliminated by rudder angle. Therefore, the final control of the AUV is attributed to the rudder angle control.

The goal of the homing control is to reduce Δy and $\Delta\psi_{\mathrm{AUV}}$ to the greatest extent possible. Generally, the PID controller includes outer loop and inner loop control. The equivalent angle of the cross-track error $\Delta\varphi'$, and AUV heading error $\Delta\psi_{\mathrm{AUV}}$ are put into the outer loop controller to obtain an equivalent heading angle Δe (Fig. 12). The input of inner loop control Δe is

$$\Delta e = k_1\Delta\varphi' + k_2\Delta\psi_{\mathrm{AUV}}, \tag{12}$$

where k_1 and k_2 are the weight coefficients of cross-track error and AUV heading error. The expressions of cross-track error Δy, the equivalent angle of the cross-track error $\Delta\varphi'$ and AUV heading error $\Delta\psi_{\mathrm{AUV}}$ are shown in (13), (14) and (15).

$$\Delta y = \left(x_{\mathrm{AUV}} - x_{\mathrm{dock}}\right)\cos\varphi_{\mathrm{dock}} - \left(y_{\mathrm{AUV}} - y_{\mathrm{dock}}\right)\sin\varphi_{\mathrm{dock}}, \tag{13}$$

$$\Delta\varphi' = \mathrm{actan}(\Delta y), \tag{14}$$

$$\Delta\psi_{\mathrm{AUV}} = \psi_{\mathrm{AUV}} - \varphi_{\mathrm{dock}}. \tag{15}$$

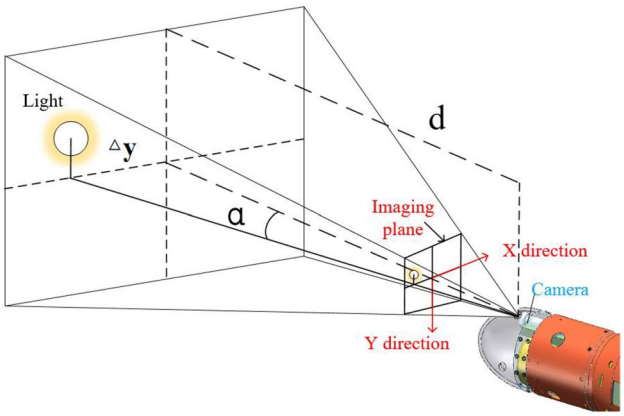

Fig. 13 Coordinate of the optical imaging system

The equivalent heading angle Δe is input into the inner loop, and it outputs the rudder angle acting directly on the AUV propulsion system. Finally, the change in the rudder angle is used to eliminate the cross-track error and AUV heading error, making the AUV close to the dock centerline and facing the funnel-type center.

5.2 Optical navigation

USBL has the disadvantage of slow updating and limited positioning accuracy. It is thus necessary to adopt optical navigation when the AUV is close to the docking station. The solution adopted is to use optical navigation when the distance between the AUV and the docking station is 20 m. The optical navigation system consists mainly of a light on the docking station, a camera on the head of the AUV, and a video data processing module (DSP).

The schematic diagram of the light imaging principle is presented in Fig. 13. Assume that the camera's central axis coincides with the central axis of the AUV. The horizontal and vertical distance from the light to the central axis of the AUV is proportional to the coordinates of the imaging point of the light. d denotes the horizontal distance between the light center and the camera, and α denotes the angle between the line that connects light center and camera and y plane (Fig. 13). Optical navigation using one camera and one light was mentioned in a previous work [37], where the coordinate information of the light is applied in PID to control the movement of the AUV both in the vertical and horizontal planes. Optical navigation in this article aims to let the AUV travel toward the light center to reduce the cross-track error along the x-direction during the AUV docking process close to the docking station. After the camera captures the light, image processing is completed by the DSP, and the coordinate information of the light central point (x_l, y_l) is generated. The information x_l is fed back into the PID controller to control the AUV rudder angle, making the AUV close to the dock centerline.

6 Control and monitoring system

The control and monitoring system is an important hub that combines the above systems correctly. The overall framework of the system is shown in Fig. 14. The core of the control and monitoring system is the embedded PC installed in the circuit chamber. We developed communication software in the host computer that can be manipulated to monitor and control this underwater docking system.

6.1 Monitoring system

According to the monitoring objects, the monitoring system can be divided into an internal monitoring module and an external monitoring module. Internal monitoring objects include humidity in the circuit chamber and voltage and current in the ICPT system. The detection of external objects is mainly monitored by external sensors. The ocean currents information near the docking station is obtained by ADCP. The attitude information of the docking station is detected by a magnetic compass (TCM5). The depth information is collected by a depth sensor installed on the inside of the end cap of the circuit chamber. The cameras located at the mainframe and the base of the docking station can display the docking process and information around the docking station on the host computer screen. The information displayed on the host computer is utilized to make corresponding control decisions, and some monitoring parameters are transmitted to the AUV in the homing and docking process.

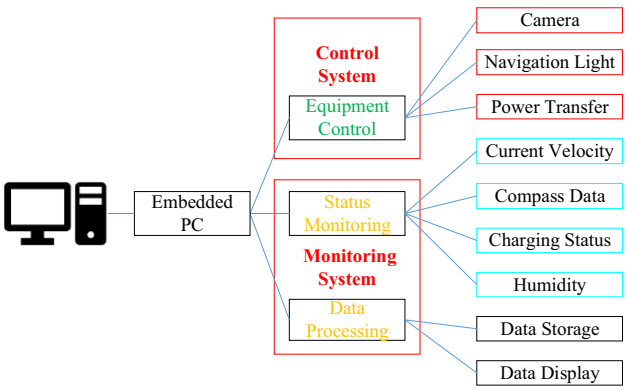

Fig. 14 The relationship between each device and the host computer

6.2 Control system

The main function of the control system is to control the opening or closing of some devices through the host computer interface to complete the AUV docking, charging, wireless communication and undocking. The entire process is shown in Fig. 15. During the docking process, the host computer connected to the docking station controls the light opening for optical navigation, simultaneously turning on the camera and

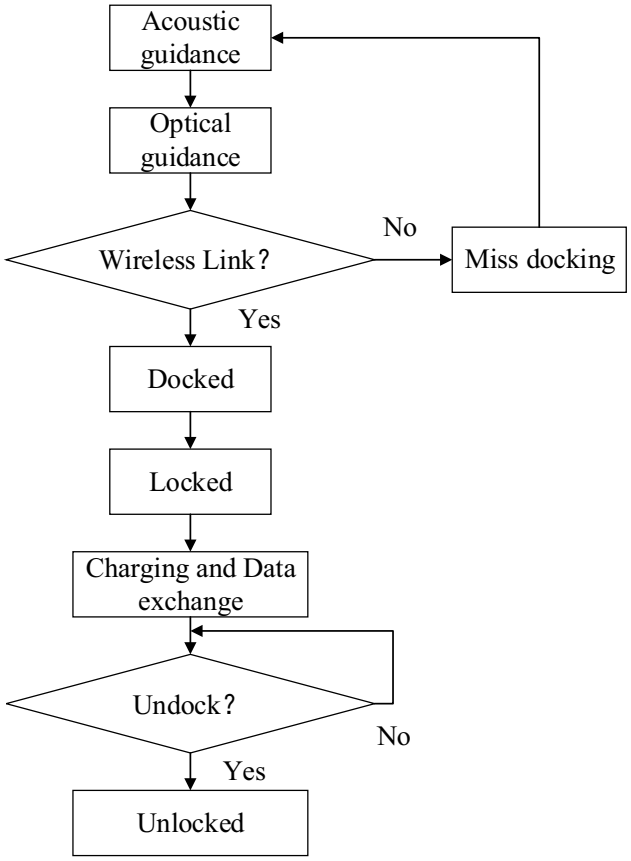

Fig. 15 Docking and undocking process

observing the AUV docking situation. When the AUV's nose smoothly enters the funnel-type entrance, the network on both sides forms an effective link that triggers the electromagnet lock, so the AUV is latched in the docking station. After the status of the AUV locked in the docking station is confirmed, data exchange and power transfer can be carried out. During AUV undocking, the electromagnet lock is controlled to be unlocked, and then the AUV reverses its propeller and starts new missions.

7 Sea trial results

In May 2017, this underwater docking system was tested in 50- and 105-m-depth sea trial. The sea state in the 50-m-depth sea trial was grade 3 [38], and the ocean currents in the experimental area were 0.403 m/s. The sea state in the 105-m-depth sea trial was grade 2 [38], and the ocean currents in the experimental area were 0.229 m/s. The docking system tested is shown in Fig. 16. During the sea trials, the underwater docking system did not connect to the COON. The power supply and the host computer were connected to it through photoelectric composite cable, a photoelectric conversion chamber and watertight cable. This sea trial verified the feasibility of the navigation system, the non-contact power transfer system, the wireless communication system and the control and monitoring system.

7.1 Results of the navigation system test

The navigation system is a key module in the docking system. Through the navigation system, successful homing and docking are related to the implementation of follow-up tasks. The AUV first spirally submerged from the surface of the water to the specified depth, reached points P1 and started the homing and docking process. Totally, 13 missions were carried out in the sea trial, and 11 of them were successfully completed. Among them, the docking system carried out 12 missions of homing and docking at the 50-m-depth area. Ten successful dockings were obtained. At the 105-m-depth area, one mission was carried out and it was also successfully completed. Because the environment of each experiment in the same sea area was similar, the trajectories of successful dockings were also similar (Fig. 17). The third experiment in the 50-m-depth area and the experiment in the 105-m-depth area are analyzed here as common cases (Figs. 18, 19, 20, and 21). The trajectories of the successful homing are shown in Fig. 18 left and Fig. 20 left. The red lines in the pictures (Fig. 18 right and Fig. 20 right) present the depth of the funnel-type entrance center. The sea floor is 3.25 m deeper than the depth shown. During the homing progress, the AUV started with acoustic navigation. Under the influence of the cross-track error control, the AUV rapidly approached the dock centerline at the beginning and then traveled near the dock centerline. The cross-track error and the heading angle error are controlled to fluctuating near the desired

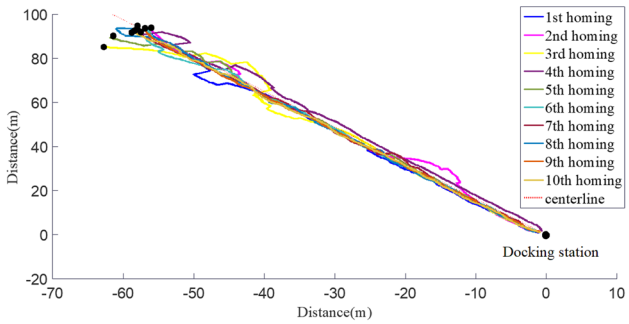

Fig. 17 Ten successful trajectories in the 50-m-depth sea area

Fig. 16 The docking station and AUV in the sea trials (left: the dock; right: the AUV)

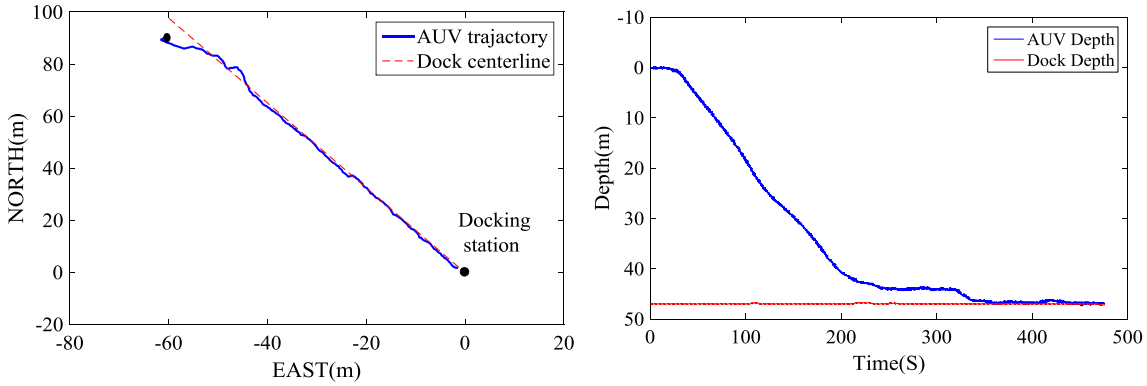

Fig. 18 Trajectory of a successful homing in the 50-m-depth sea area (left: the trajectory of the AUV; right: the depth of the docking station and AUV). (Color figure online)

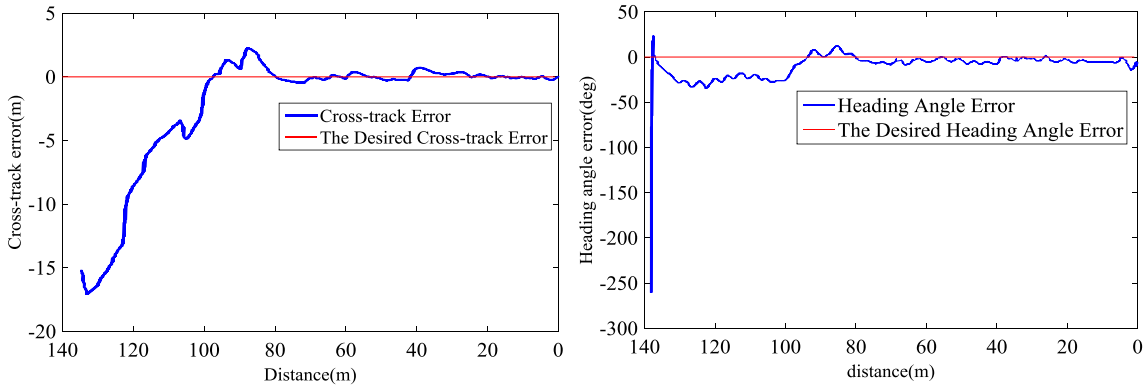

Fig. 19 The cross-track error and heading angle error of the AUV in the third experiment in the 50-m-depth sea area (left: the cross-track error; right: the heading angle error)

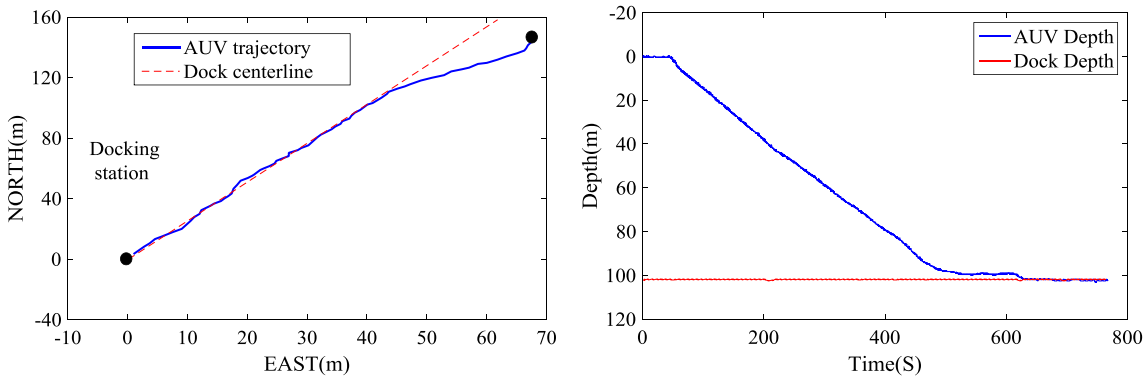

Fig. 20 Trajectory of a successful homing in the 105-m-depth sea area (left: the trajectory of the AUV; right: the depth of the docking station and AUV). (Color figure online)

value (Figs.19, 21). When its distance to the docking station reached 20 m, optical navigation worked. The result of the process of optical navigation is shown in Fig. 22. Guided by the light, the AUV docked into the funnel-type entrance successfully.

7.2 Results of the non-contact power transfer system test

The underwater non-contact power transfer system is the premise for improving the endurance of the AUV. During

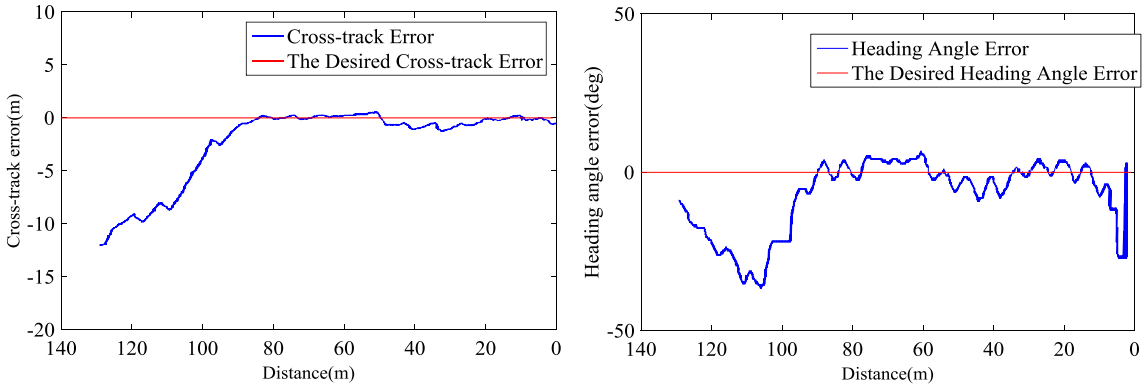

Fig. 21 The cross-track error and heading angle error of the AUV in the third experiment in 105-m-depth sea area (left: the cross-track error; right: the heading angle error)

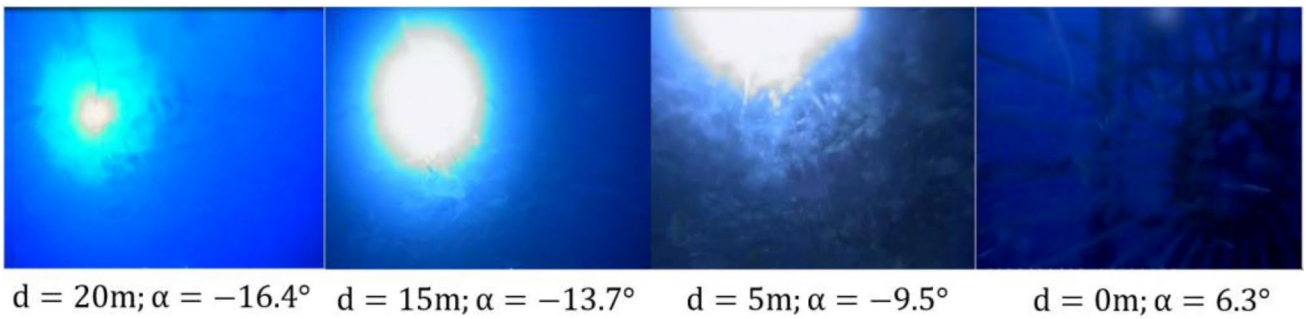

Fig. 22 Pictures captured by the camera in front of the AUV during optical navigation (the first data under each image is the distance between the light and the camera in the horizontal direction. The second one is the angle between the y plane of the imaging coordinate system and the line that connects the light center and the camera)

the sea trial, the N5772A and N8742A KEYSIGHT power sources were applied to supply 375 V DC power to the docking station and the ICPT system, respectively. The voltage and current of the ICPT system were displayed on the host computer interface. The maximum charging power was 682 W, and the total efficiency and the efficiency of the power transfer unit were 78.5% and 92%, respectively (Fig. 23). With the continuous transmission of electrical energy, both the output voltage of the secondary side (V_o) and the battery (V_{bat}) rose gently. The data of the power and voltage of the secondary side during charging is obtained. The equivalent resistance (R_e) and theoretical power of the secondary side can be calculated out. In the theoretical analysis, we used the fundamental analysis method that the harmonic component is ignored. Also, the relationship of the voltage across the rectifier is approximated. So the theoretical power of the secondary output is slightly lower than the actual power of the secondary output (Fig. 23).

7.3 Results of the wireless communication system test

Wireless communication is the task that needs to be executed after the AUV enters the dock. During sea trial, a file transfer protocol (FTP) server was used to detect the data transmission rate, and file sizes of 106 MB and 700 MB were exchanged between the docking station and the AUV. We define the upload as files transfer from the docking station to the AUV. The results of wireless communication are shown in Table 2. Files of 106 MB and 700 MB were uploaded to the AUV at stable rates of 1.8 MB/s and 3.1 MB/s, respectively. Files of 700 MB were downloaded at a rate of 1.5 MB/s. The reason why the rates were different is that the AUV was fixed in the docking station with different roll angles which lead to the different distance between the two antennas in the docking station and the AUV. When the roll angle is close to 0°, the distance between the two antennas is shorter, so the transmission rate is relatively higher. The transmission rates at three different antenna distances

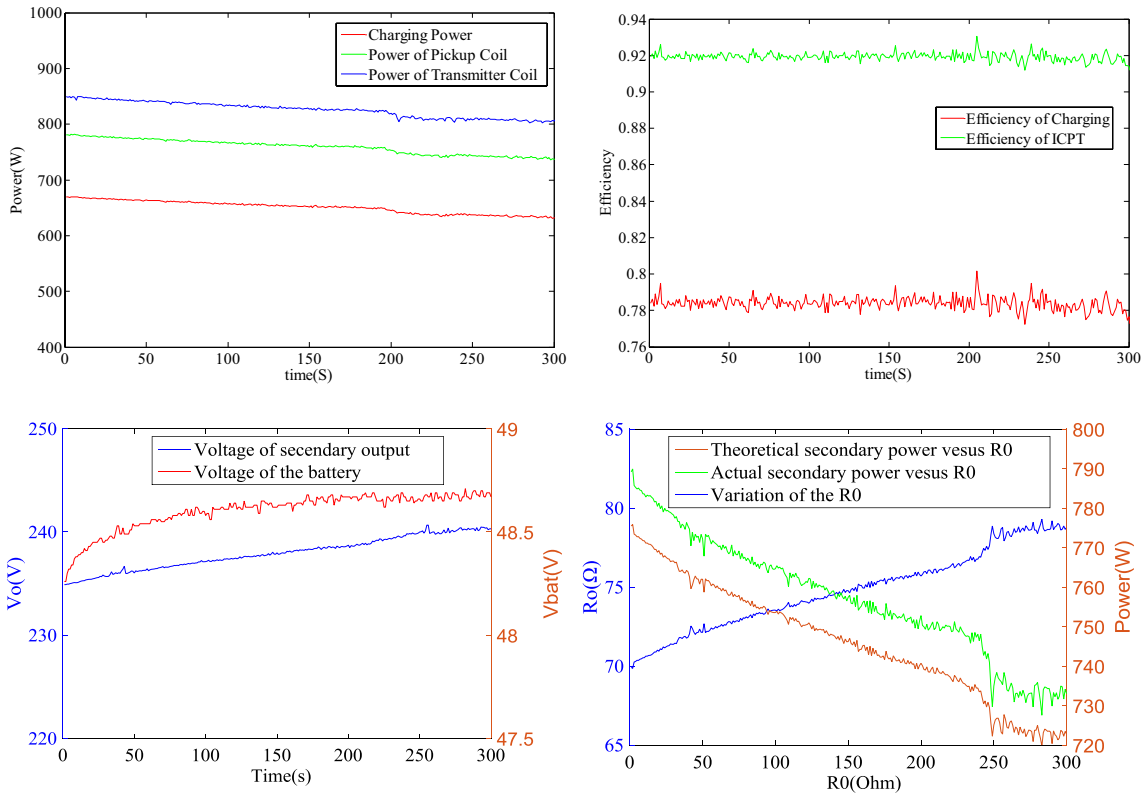

Fig. 23 Results of power transfer test (upper left: the power; upper right: the efficiency; bottom left: the voltage of the secondary side and the battery; bottom right: compare between the actual and theoretical power of the secondary output versus different equivalent resistance of the secondary output)

Table 2 Result of wireless communication test

File size (MB)	Rate (MB/s)	Upload or download	AUV roll angle (°)	Distance between antennas (mm)
106	1.8	Upload	−24	60
700	3.1	Upload	7	42
700	1.5	Download	−26	63

(3.1 MB/s, 1.8 Mb/s, 1.7 Mb/s) are slightly lower than those in Fig. 6 (3.5 MB/s, 2.0 Mb/s, 1.85 MB/s). On the one hand, the equipment in the network architecture during the sea trial was different from the equipment used in the laboratory testing. On the other hand, while transferring large files, the controller in the docking station also transmitted new tasks to the AUV, so that the measured transmission rate would be lower than the results in Fig. 6. Generally speaking, the results of the sea trial are in line with the trend of transmission rate in Fig. 6.

7.4 Results of the control and monitoring system test

The control and monitoring system controlled the various tasks of the docking station and displayed and recorded the collected data from various sensors. The operator manipulated some tasks during the docking and undocking process through the interface on the host computer, such as turning the light on or off, using the electromagnetic lock, video detection and charging. In addition, the humidity status of the circuit chamber, the attitude of the docking station, the link status of wireless communication, the parameters related to the electric energy and ocean currents data were displayed on the host computer screen. Because of the cameras installed in the docking station (Fig. 1), the status of the docking process can be spied by them in the host computer interface (Fig. 24).

Fig. 24 Docking situation captured by cameras displayed in the host computer interface (the left and right one captured by camera1 and camera2 displayed in Fig. 1, respectively. The two photos were token when the AUV successfully docked and latched in the docking station. The orange object is the AUV and the yellow one is the docking station). (Color figure online)

8 Conclusion

A prototype AUV docking system was implemented and its feasibility was verified in sea tests. All key systems, including a wireless communication system, a non-contact power transfer system, a navigation system and a control and monitoring system performed well. Adopting the combined use of acoustic and optical navigation, the AUV achieved precise homing and docking. High-speed underwater wireless communication was achieved by using high-frequency electromagnetic wave communication technology. Based on the inductively coupled power transfer system, high-power and high-efficiency charging was completed. The host computer and embedded PC controller in the docking station were used in conjunction to build an effective control and monitoring system. The compatibility of all systems and the reliability of their working together have been validated. However, the system still has many limitations. During the experiments, the ship's power supply and Ethernet were used to simulate the COON to provide power and communication interfaces to the docking system. The system is now used to carry out docking missions around 100 m. The navigation control methods should be improved to achieve remoter homing missions. Moreover, for the first time, this docking system has realized complete navigation, wireless communication and charging in a depth of more than 100 m, laying a promising foundation for the joint use of the COON and AUV. How to improve the battery capacity and charging power of AUV, how to achieve remoter homing and docking navigation and how to improve the navigation accuracy will be the focus of future work.

Acknowledgements The authors appreciate the financial support from the National High Technology Research and Development Program of China (No. 2013AA09A414) and the National Natural Science Foundation of China (No. 41676089).

References

1. Barnes CR, Best M, Johnson FR, NEPTUNE Canada (2015) Installation and initial operation of the world's first regional cabled ocean observatory. Springer, Berlin
2. Podder T, Sibenac M, Bellingham J (2004) AUV docking system for sustainable science missions. In: IEEE international conference on robotics and automation, pp 4478–4485
3. Nicholson J, Healey A (2008) The present state of autonomous underwater vehicle (AUV) applications and technologies. Mar Technol Soc J 42(1):44–51
4. M MNA (2012) Design of a docking station for autonomous underwater vehicles (AUV) recharge and data download. Instrum Viewp 4(28):28–29
5. Skomal GB et al (2015) Subsurface observations of white shark Carcharodon carcharias predatory behaviour using an autonomous underwater vehicle. J Fish Biol 87(6SI):1293–1312
6. Singh H et al (2001) Docking for an autonomous ocean sampling network. IEEE J Ocean Eng 26(4):498–514
7. Fukasawa T, Noguchi T, Kawasaki T (2003) "MARINE BIRD", a new experimental AUV with underwater docking and recharging system. Oceans 4:2195–2200
8. Lambiotte JC et al (2002) Results from mechanical docking tests of a Morpheus class AUV with a dock designed for an OEX class AUV. Oceans'02 MTS/IEEE 1:260–265
9. Zhang T, Li D, Yang C (2017) Study on impact process of AUV underwater docking with a cone-shaped dock. Ocean Eng 130:176–187
10. Stokey R, Purcell M, Forrester N (1997) A docking system for REMUS, an autonomous underwater vehicle. Oceans 2:1132–1136
11. Allen B et al (2006) Autonomous docking demonstrations with enhanced REMUS technology. Oceans-IEEE 1539
12. Stokey R et al (2001) Enabling technologies for REMUS docking: an integral component of an autonomous ocean-sampling network. IEEE J Ocean Eng 26(4):487–497
13. McEwen RS et al (2008) Docking control system for a 54-cm-diameter (21-in) AUV. IEEE J Ocean Eng 33(4):550–562

14. Hobson BW, McEwen RS (2007) The development and ocean testing of an AUV. Oceans 29:1–6
15. Coulson R, Lambiotte J, An E (2005) A modular docking system for 12.75-inch class AUVs—a funnel-type dock using inductive power transfer and a radio frequency ethernet bridge. Sea Technol 46(4):49–54
16. Brighenti A et al (1998) EURODOCKER—a universal docking-downloading-recharging system for AUVs: conceptual design results. Oceans'98 Conf Proc 3:1463–1467
17. Podder T, Sibenac M, Bellingham J (2004) AUV docking system for sustainable science missions. Robot Autom 5:4478–4484
18. Kojiya T et al (2004) Automatic power supply system to underwater vehicles utilizing non-contacting technology. Oceans'04 4:2341–2345
19. Han J et al (2006) High speed acoustic network and noncontact power supplier for seafloor geodetic observing robot system
20. Han J et al (2007) Noncontact power supply for seafloor geodetic observing robot system. J Mar Sci Technol 12(3):183–189
21. Feezor MD, Sorrell FY, Blankinship PR (2001) An interface system for autonomous undersea vehicles. IEEE J Ocean Eng 26(4):522–525
22. Bradley AM et al (2001) Power systems for autonomous underwater vehicles. IEEE J Ocean Eng 26(4):526–538
23. Li DJ et al (2015) Autonomous underwater vehicle docking system for cabled ocean observatory network. Ocean Eng 109:127–134
24. Shi JG, Li DJ, Yang CJ (2014) Design and analysis of an underwater inductive coupling power transfer system for autonomous underwater vehicle docking applications. Front Inf Technol Electron Eng 15(1):51–62
25. Lacovara P (2008) High-bandwidth underwater communications. Mar Technol Soc J 42(1):93–102
26. B B (2004) A low power a, low cost, underwater optical communication system. Ridge 2000 Events
27. Sozer EM, Stojanovic M, Proakis JG (2000) UAN—underwater acoustic network. IEEE J Ocean Eng 42(1):72–83
28. Iizuka K (1963) An experimental study of the insulated dipole antenna immersed in a conducting medium. IEEE Trans Antennas Propag 11(5):518–532
29. Siegel M, King R (1973) Electromagnetic propagation between antennas submerged in the ocean. IEEE Trans Antennas Propag 21(4):507–513
30. Al-Shamma'a AI, Shaw A, Saman S (2004) Propagation of electromagnetic waves at MHz frequencies through seawater. IEEE Trans Antennas Propag 52(11):2843–2849
31. Kazmierkowski MP, Moradewicz AJ (2012) Contactless energy transfer (CET) systems—a review. 2012 15th international power electronics and motion control conference (EPE/PEMC)
32. Kim Y, Jin K (2012) A contactless power transfer system using a series–series–parallel resonant converter. Int J Electron 99:885–897
33. Villa JL et al (2012) High-misalignment tolerant compensation topology for ICPT systems. IEEE Trans Ind Electron 59:945
34. Wang CS, Covic G, Stielau OH (2004) Power transfer capability and bifurcation phenomena of loosely coupled inductive power transfer systems. IEEE Trans Ind Electron 51:148–157
35. Rim CT, Cho GH (1990) Phasor transformation and its application to the DC/AC analyses of frequency phase-controlled series resonant converters (SRC). IEEE Trans Power Electron 5(2):201–211
36. Vickery K (1998) Acoustic positioning systems a practical overview of current systems, pp 5–17
37. Li D, Zhang T, Yang C (2016) Terminal underwater docking of an autonomous underwater vehicle using one camera and one light. Mar Technol Soc J 50(6):58–68
38. Parvaresh A, Hassanzadeh S, Bordbar MH (2005) Statistical analysis of wave parameters in the north coast of the Persian Gulf. Ann Geophys 23(6):2031–2038